Crystal chemistry rationale and ab initio investigation of ultra-hard dense rhombohedral carbon and boron nitride

Samir Matar, Vladimir Solozhenko

Crystal chemistry rationale and *ab initio* investigation of ultra-hard dense rhombohedral carbon and boron nitride

Samir F. Matar [1,§,*] and Vladimir L. Solozhenko [2]

[1] Lebanese German University (LGU), Sahel Alma, Jounieh, Lebanon

https://orcid.org/0000-0001-5419-358X

[2] LSPM–CNRS, Université Sorbonne Paris Nord, 93430 Villetaneuse, France

https://orcid.org/0000-0002-0881-9761

[§] *Former DR1-CNRS senior researcher at the University of Bordeaux, ICMCB-CNRS, France*

[*] Corresponding author email: s.matar@lgu.edu.lb and abouliess@gmail.com

Abstract

Rhombohedral dense forms of carbon, rh-C_2 (or hexagonal h-C_6), and boron nitride, rh-BN (or hexagonal h-B_3N_3), are derived from rhombohedral 3R graphite based on original crystal chemistry scheme backed with full cell geometry optimization to minimal energy ground state computations within the quantum density functional theory. Considering throughout hexagonal settings featuring extended lattices, the calculation of the hexagonal set of elastic constants, provide results of large bulk moduli i.e. B_0(rh-C_2) = 438 GPa close to that of diamond, and B_0(rh-BN) = 369 GPa close to that of cubic BN. The hardness assessment in the framework of three contemporary models enables both phases to be considered as ultra-hard. From the electronic band structures calculated in the hexagonal Brillouin zones, 3R graphite is a small-gap semiconductor, oppositely to rh-C_2 that is characterized by a large band gap close to 5 eV, as well as the two BN phases.

Keywords: DFT; superhard materials; dimensionality, carbon; boron nitride

Dedication:

In memoriam of Prof. Gérard Demazeau (University of Bordeaux-France). † November 2017

1- Introduction and crystal chemistry rationale

Graphite is mainly known as 2*H* structure with two carbon layers in hexagonal $P6_3/mmc$ space group. Nevertheless, early crystal structure analyses of natural graphite by Lipson and Stokes [1, 2] showed the occurrence of extra lines in its X-ray pattern. The hypothesis of impurity was rapidly discarded, and the authors concluded to the presence of a non negligible percentage of a rhombohedral phase called 3*R* graphite in $R\bar{3}m$ space group. The structure shown in Fig. 1a using hexagonal axes (for a better presentation than with a rhombohedron) is characterized by 3 layers. Both hexagonal and rhombohedral graphite exhibit a triangular planar coordination of sp^2 carbon with an angle of 120°. In 2*H* graphite the carbon atoms occupying the two layers are in fixed Wyckoff positions, i.e. C1 at 2*b* (0, 0, ¼) and C2 at 2*c* (1/3, 2/3, ¼). Oppositely, in 3*R* graphite (three layers) there is one carbon equivalent at the special twofold 2*c* (*x, x, x*) Wyckoff position of $R\bar{3}m$ space group. By using hexagonal axes, the atoms are in the six-fold position 6*c* (0, 0, *z*). With $z = 0.164$ a closer agreement with the X-ray intensities was obtained, leading to a slight ±0.03Å out-of-plane displacement of atoms, i.e. with puckered layers whereas with $z = 0.167$ (1/6) a planar configuration is kept [1]. Then allowing changes in *z* with different magnitudes below 1/6 induces departures from the co-planarity of C atoms to increasingly puckered layers leading eventually to a 3D atomic arrangement alike in diamond as shown here below. A lowering of *z* from 0.164 down to 0.125 let obtain an intermediate structure shown in Fig. 1b accompanied by a change of ∠C-C-C angle from 120° characteristic of sp^2-carbon (Fig. 1a) down to 96°. The resulting constrained structure was then submitted to full geometry relaxation using quantum density functional theory (DFT) calculations [3, 4] (cf. next section), leading to ∠C-C-C = 109.47° characteristic of C(sp^3) and a smaller volume . The relaxed structure in Fig. 1c presents a succession of corner sharing *C4* tetrahedra in a diamond-like manner.

Extending the crystal chemistry mechanism to boron nitride, a similar approach was adopted with the difference of a lowering of the symmetry from $R\bar{3}m$ (space group No 166) *to* *R*3*m* (space group N° 160) due to the occupation of the 2*c* (*x, x, x*) position - or 6*c* (0, 0, *z*) -, by two different chemical species, B and N. A rhombohedral BN predicted from *ab initio* simulated annealing was cited in 2008 [5]. The structure shown in Fig. 2i was subsequently calculated with ground state energy close to the new 3*R* graphitic BN (Table 1) obtained from the carbon analogue (Fig. 1a). However we did not retain it as model for present study due to the large difference of structural arrangement of the layers with respect to the model derived from 3*R* C_2 which leads to 3*R* BN sketched in Fig. 2a. This model followed in the representations in Fig. 2b, and Fig. 2c indicates a mechanism of structure transformation closely resembling the one used for carbon.

2- Computational framework

The search for C and BN ground state structures and calculations of energies of the different phases were based on DFT within the plane-wave Vienna Ab initio Simulation Package VASP code [6, 7] used with the projector augmented wave (PAW) method [7,8] for the atomic potentials with all valence states, especially, in regard of such light elements as B and N. The effects of exchange-correlation were accounted for calling for the generalized gradient approximation (GGA) [9]. A conjugate-gradient algorithm according to Press *et al*. [10] was used in this computational scheme to relax the atoms onto the ground state. The tetrahedron method with Blöchl *et al*. corrections [11] and Methfessel-Paxton scheme [12] were applied for both geometry relaxation and total energy calculations. Brillouin-zone (BZ) integrals were approximated using a special **k**-point sampling of Monkhorst and Pack [13]. The optimization of the structural parameters was performed until the forces on the atoms were less than 0.02 eV/Å, and all stress components less than 0.003 eV/Å^3. The calculations were converged at an energy cut-off of 500 eV for the plane-wave basis set concerning the **k**-point integration in the Brillouin zone, with a starting mesh of 6×6×6 up to 12×12×12 for best convergence and relaxation to zero strains. In the post-treatment process of the ground state electronic structures, the charge density and the electronic band structures are computed and illustrated. The mechanical properties were derived from the calculation of the elastic constants C_{ij} in the hexagonal system.

3- Calculations and results.

3-1. *Crystal structures using hexagonal setting.*

From full geometry relaxation and ground state energies, Table 1 provides the resulting crystal parameters and the corresponding energies for all C_6 and B_3N_3 structures. For graphitic C_6 the experimental [1] and calculated data provided in the first two columns exhibit slight differences for *a* and *c* lattice constants, especially, for a larger calculated *c*. The starting $z_C = 0.164$ changes to 1/6, thus showing that planar carbon arrangement is favored energetically *versus* puckered layers structure. Agreement with experiment is also found for the interatomic distance d(C-C) = 1.42 Å.

Confronted with 2*H* graphite, the total energy for 4 C (note *i* at the bottom of Table 1) is very close to 3*R* C2 total energy. 3D *rh*-C_2 on the other hand is characterized by a slightly higher total energy, and its energy is equal to that of diamond and is less than that of lonsdaleite (hexagonal diamond) – indicated in note *j*.

Turning to BN phases, the same trend of slightly higher 3D *rh*-BN *versus* 3*R* BN is noted, the latter being at energy close to 3*R* BN [5] – note *k*. The total energy values are mirrored by the trends of cohesive energies given at the last line of Table 1. Regarding the crystal structures, the 2D phases are characterized by systematically larger *c* hexagonal parameters whilst *a* planar lattice constant changes much less, and the 2D phases are characterized by $z_{C;B;N} = 0.167 / 0.833$, while the 3D phases have $z_{C;B;N} = 0.125 / 0.875$. Finally, the shortest distances are smaller in 2D phases due to in-

plane binding within the layer, and larger in 3D phases where the distance describes the *C4* tetrahedron (Fig. 1c) or *BN3* / *NB3* tetrahedra in Fig. 2c.

3-2. *Charge density*

To further assess the electronic and crystal structure relationship, the charge density projections onto the chemical constituents as situated in the crystal lattice are needed. Fig. 3a shows the charge density (yellow) volumes in 3*R* graphite expressed in three layers within continuous yellow rings of sp^2-like C. Oppositely in Fig. 3b the charge density around carbon atoms in *rh*-C_2 (C_6 in hexagonal coordinates) shows a perfect sp^3 tetrahedral shape carbon charge density arranged into tetrahedra reproducing the structure sketch in Fig. 1c.

Clearly, the two carbon compounds are perfectly covalent chemical systems because of the presence of one chemical species, C, with electronegativity $\chi C = 2.55$. The situation becomes less obvious upon accounting for BN where $\chi B = 2.04$ is much lower than $\chi N = 3.04$. The larger electronegativity of N leads to a charge transfer B→N resulting in charge-poor B and charge-rich N as illustrated in next paragraph. The 3*R* BN charge density in Fig. 3c illustrates the polar covalent chemical behavior with the charge pointing from N towards B with an ovoid shape especially visible in the middle layer. In Fig. 3d showing the charge density of 3D *rh*-BN, the tetrahedral arrangement which is similar to Fig. 3b of 3D carbon analogue is visible on N charge density, especially, in the *B3N* tetrahedron at the lower part of the figure.

3-3. *Electronic band structures*

Figure 4 shows the electronic band structures along the main directions of the first wedge in rhombohedral Brillouin zones. All four carbon phases possess band gaps separating the filled valence band (VB) from the empty conduction band (CB), so that the zero of energy along the *y*-axis is at E_V top of the valence band.

In 2D carbon, the gap is very small in agreement with a semi-conducting character. Oppositely, the 3D carbon phase has a large band gap, indirect, with a value close to 5 eV. This is also observed in the 3D BN phase with a slightly lower band gap of 5 eV. The iono-covalent character brought by the presence of two chemical elements with different electronegativities is exhibited in the band structure of 3D BN where the s-like bands due to nitrogen are below -15 eV and well separated from the p block above this energy. Both 3D phases are considered as large band gap insulators, one covalent and the other iono-covalent.

3-4. *Mechanical properties.*

The assessment of the mechanical properties is based on the elastic properties determined by performing finite distortions of the lattice and deriving the elastic constants from the strain-stress relationship.

In hexagonal symmetry there are six independent elastic stiffness constants C_{11}, C_{33}, C_{44}, C_{12}, and C_{13}. Most compounds are encountered in polycrystalline form where one may consider the single crystalline grains randomly oriented. Consequently on a large scale, such materials can be considered as statistically isotropic. They are then fully described by the bulk modulus *B* and the shear modulus *G* that may be obtained by averaging the single-crystal elastic constants. A widely used averaging method of elastic constants is Voigt's one [14] based on a uniform strain. The calculated set of elastic constants (in GPa) are:

rh-C_2	$C_{11} = 1117$;	$C_{12} = 93$;	$C_{13} = 61$;	$C_{33} = 1280$;	$C_{44} = 510$.
rh-BN	$C_{11} = 915$;	$C_{12} = 119$;	$C_{13} = 74$;	$C_{33} = 960$;	$C_{44} = 352$.

All C_{ij} values are positive and their combinations: $C_{11} > C_{12}$, $C_{11}C_{33} > C_{13}^2$ and $(C_{11}+C_{12})C_{33} > 2C_{13}^2$ obey the rules pertaining to the mechanical stability of the phase.

The bulk (B_V) and shear (G_V) moduli following Voigt are formulated as:

$$B_V = 1/9\ \{2(C_{11} + C_{12}) + 4C_{13} + C_{33}\},$$

and

$$G_V = 1/30\ \{C_{11} + C_{12} + 2\ C_{33} - 4C_{13} + 12\ C_{44} + 6(C_{11} - C_{12})\}$$

The calculated moduli are then as follows:

rh-C_2: $B_V = 438$ GPa, $G_V = 542$ GPa

rh-BN: $B_V = 369$ GPa, $G_V = 389$ GPa

These results are in close agreement with corresponding values of diamond and *c*-BN (see Tables 2b and 3b).

Vickers hardness (H_V) was predicted using three contemporary theoretical models of hardness: (i) Mazhnik-Oganov model [15], (ii) Chen-Niu model [16], and (iii) thermodynamic model [17]. The first two models use the elastic properties, while the thermodynamic model is based on crystal structure and thermodynamic properties. Mazhnik-Oganov model was also used for the estimation of fracture toughness (K_{Ic}). The results are presented in Tables 2 and 3.

Tables 2a and 3a present Vickers hardness (H_V) and bulk moduli (B_0) calculated in the framework of the thermodynamic model of hardness, and Tables 2b and 3b present the other mechanical properties such as shear modulus (G), Young's modulus (E), the Poisson's ratio (ν) and fracture toughness (K_{Ic}).

A slightly higher hardness of rhombohedral carbon compared to diamond (both cubic and hexagonal) is observed for all three models (Table 2a). The similar trend is also found for the dense rhombohedral boron nitride *versus* cubic and wurtzite polymorphs. A good agreement is observed for the bulk moduli estimated using the thermodynamic model (B_0) with the values calculated from the set of elastic constants (B_V).

In general, both *rh*-C_2 and *rh*-BN have superior mechanical properties and thus can be considered as prospective ultra-hard materials [28].

4- Conclusion

Crystal chemistry rationale of structurally transforming rhombohedral graphitic carbon and boron nitride into three dimensional dense forms was followed by geometry-optimization calculations within DFT. The ground state energies of 3D structures of *rh*-C_2 (or *h*-C_6**)** and *rh*-BN **(**or *h*-B_3N_3**)** were determined as well as the energy-related physical quantities as elastic constants, charge density and electronic band structures. Compared to diamond and lonsdaleite, *rh*-C_2 is shown to possess slightly better mechanical properties such as hardness and fracture toughness. Also, *rh*-BN shows hardness value close to those of superhard cubic boron nitride.

References

[1] Lipson, H.; Stokes, A.R. The structure of graphite. *Proc. R. Soc. Lond., Series A*, **181** (1942) 101-105.

[2] Lipson, H.; Stokes, A.R. A new structure of carbon. *Nature*, **149** (1942) 328.

[3] Hohenberg, P.; Kohn, W. Inhomogeneous electron gas. *Phys. Rev. B*, **136** (1964) 864−871.

[4] Kohn, W.; Sham, L.J. Self-consistent equations including exchange and correlation effects. *Phys. Rev. A*, **140** (1965) 1133−1138.

[5] Doll, K.; Schoen, J.C.; Jansen, M. Structure prediction based on *ab initio* simulated annealing for boron nitride. *Phys. Rev. B*, **78** (2008) 144110.

[6] Kresse, G.; Furthmüller, J. Efficient iterative schemes for ab initio total-energy calculations using a plane-wave basis set. *Phys. Rev. B*, **54** (1996) 11169-11186.

[7] Kresse, G.; Joubert, J. From ultrasoft pseudopotentials to the projector augmented wave. *Phys. Rev. B*, **59** (1999) 1758-1775.

[8] Blöchl, P.E. Projector augmented wave method. *Phys. Rev. B*, **50** (1994) 17953-17979.

[9] Perdew, J.; Burke, K.; Ernzerhof, M. The Generalized Gradient Approximation Made Simple. *Phys. Rev. Lett.*, **77** (1996) 3865-3868.

[10] Press, W.H.; Flannery, B.P.; Teukolsky, S.A.; Vetterling, W.T. *Numerical Recipes*, 2nd ed., Cambridge University Press: New York, NY, USA, 1986.

[11] Blöchl, P.E.; Jepsen, O.; Anderson, O.K. Improved tetrahedron method for Brillouin-zone integrations. *Phys. Rev. B*, **49** (1994) 16223-16233.

[12] Methfessel, M.; Paxton, A.T. High-precision sampling for Brillouin-zone integration in metals. *Phys. Rev. B*, **40** (1989) 3616-3621.

[13] Monkhorst, H.J.; Pack, J.D. Special k-points for Brillouin zone integration. *Phys. Rev. B*, **13** (1976) 5188-5192.

[14] Voigt, W. Über die Beziehung zwischen den beiden Elasticitätsconstanten isotroper Körper, *Annal. Phys.*, **274** (1889) 573-587.

[15] Mazhnik, E.; Oganov, A.R. A model of hardness and fracture toughness of solids. *J. Appl. Phys.*, **126** (2019) 125109.

[16] Chen, X-Q.; Niu, H.; Li, D.; Li, Y. Modeling hardness of polycrystalline materials and bulk metallic glasses. *Intermetallics*, **19** (2011) 1275-1281.

[17] Mukhanov, V.A.; Kurakevych, O.O.; Solozhenko V.L. The interrelation between hardness and compressibility of substances and their structure and thermodynamic properties. *J. Superhard Mater.*, **30** (2008) 368-378.

[18] Matar, S.F.; Solozhenko, V.L. Ultra-hard rhombohedral carbon from crystal chemistry rationale and first principles. arXiv:2104.01076 (2021).

[19] Ownby, P.D.; Yang, X.; Liu, J. Calculated X-ray diffraction data for diamond polytypes. *J. Am. Ceram. Soc.*, **75** (1992) 1876-1883.

[20] Bindzus, N.; Straaso, T.; Wahlberg, N.; Becker, J.; Bjerg, L.; Lock, N.; Dippel, A.-C.; Iversen, B.B. Experimental determination of core electron deformation in diamond. *Acta Cryst.*, **A70** (2014) 39-48.

[21] Brazhkin, V.V.; Solozhenko V.L. Myths about new ultrahard phases: Why materials that are significantly superior to diamond in elastic moduli and hardness are impossible. *J. Appl. Phys.*, **125** (2019) 130901.

[22] Matar, S.F.; Solozhenko, V.L. Crystal chemistry and *ab initio* prediction of ultra-hard rhombohedral B_2N_2 and BC_2N. arXiv:2103.06802 (2021).

[23] Kurdyumov, A.V.; Solozhenko, V.L.; Zelyavski W.B. Lattice parameters of boron nitride polymorphous modifications as a function of their crystal-structure perfection. *J. Appl. Cryst.*, **28** (1995) 540-545.

[24] Solozhenko, V.L.; Chernyshev, V.V.; Fetisov, G.V.; Rybakov, V.B.; Petrusha I.A. Structure analysis of the cubic boron nitride crystals. *J. Phys. Chem. Solids*, **51** (1990) 1011-1012.

[25] Solozhenko, V.L.; Häusermann, D.; Mezouar, M.; Kunz M. Equation of state of wurtzitic boron nitride to 66 GPa. *Appl. Phys. Lett.*, **72** (1998) 1691-1693.

[26] Nagakubo, A.; Ogi, H.; Sumiya, H.; Kusakabe, K.; Hirao M. Elastic constants of cubic and wurtzite boron nitrides. *Appl. Phys. Lett.*, **102** (2013) 241909.

[27] Zhang, J.S.; Bass, J.D.; Taniguchi, T.; Goncharov, A.F.; Chang, Y.-Y.; Jacobsen, S.D. Elasticity of cubic boron nitride under ambient conditions. *J. Appl. Phys.*, **109** (2011) 063521.

[28] Solozhenko, V.L.; Le Godec, Y. A hunt for ultrahard materials. *J. Appl. Phys.*, **126** (2019) 230401.

Table 1 Hexagonal setting of rhombohedral carbon (SG #166) and boron nitride (SG #160). All atoms are at (0, 0, *z*) positions. Distances are in Å and energies in eV units.

	C_6			B_3N_3	
	2D (exp)	2D	3D	2D	3D
a	2.52	2.46	2.52	2.51	2.56
c	10.21	10.64	6.17	9.65	6.27
z_C	0.164	0.167	0.125		
z_B				0.167	0.125
z_N				0.833	0.875
$d_{C\text{-}C\ (B\text{-}N)}$	1.42	1.42	1.54	1.45	1.57
E_{tot}		-55.32	-54.54	-52.59	-52.26
E_{tot}/at		-9.22 [i]	-9.09 [j]	-8.76 [k]	-8.74 [l]
E_{coh}/at		-2.75	-2.62	-2.58	-2.52

Comparative energies (eV/at.):

[i] graphite 2*H*: -9.32
[j] diamond: -9.09, lonsdaleite: -9.06
[k] B_3N_3 [5]: -8.78
[l] c–BN: -8.71

Atomic energies: *E* (C) = -6.47 eV , *E* (B) = -5.57 eV, *E* (N) = -6.8 eV

Table 2a Vickers hardness (H_V) and bulk moduli (B_0) of carbon allotropes calculated in the framework of the thermodynamic model of hardness [17]

	Space group	a (Å)	c (Å)	ρ (g/cm^3)	H_V (GPa)	B_0 (GPa)
rh-C_2	*R*-3*m*	2.5190	6.17026	3.5294	98	445
rh-C_4 [18]	*R*-3*m*	2.5004	12.2100	3.6204	100	456
Lonsdaleite	*P*63/*mmc*	2.5221†	4.1186†	3.5164	97	443
Diamond	*Fd*-3*m*	3.56661‡	–	3.5169	98	445§

† Ref. 19

‡ Ref. 20

§ Ref. 21

Table 2b Mechanical properties of carbon allotropes: Vickers hardness (H_V), bulk modulus (B_0), shear modulus (G), Young's modulus (E), Poisson's ratio (ν) and fracture toughness (K_{Ic})

	H_V			B		G	E §	ν §	K_{Ic} †
	T*	MO†	CN‡	B_0 *	B_V				
	GPa								MPa·m^{½}
rh-C_2	98	103	99	445	438	542 (G_V)	1151	0.062	6.4
rh-C_4 [18]	100	105	97	456	458	552 (G_V)	1181	0.070	6.7
Lonsdaleite	97	99	94	443	432	521 (G_V)	1115	0.070	6.2
Diamond	98	100	93	445**		530**	1138	0.074	6.4

* Thermodynamic model [17]

† Mazhnik-Oganov model [15]

‡ Chen-Niu model [16]

§ E and ν values calculated using isotropic approximation

** Ref. 21

Table 3a Vickers hardness (H_V) and bulk moduli (B_0) of dense BN polymorphs calculated in the framework of the thermodynamic model of hardness [17]

	Space group	*a* (Å)	*c* (Å)	ρ (g/cm^3)	H_V (GPa)	B_0 (GPa)
rh-BN	*R*-3*m*	2.54365	6.24479	3.5361	56	382
rh-B_2N_2 [22]	*R*-3*m*	2.5004	12.24821	3.4691	55	375
w-BN	*P*63/*mc*	2.5505†	4.210†	3.4756	54	374
c-BN	*F*-43*m*	3.6160‡	–	3.4869	55	377§

† Ref. 23

‡ Ref. 24

§ Ref. 25

Table 3b Mechanical properties of dense BN polymorphs: Vickers hardness (H_V), bulk modulus (B_0), shear modulus (G), Young's modulus (E), Poisson's ratio (ν) and fracture toughness (K_{Ic})

	H_V			B		G	E [§]	ν [§]	K_{Ic} [†]
	T[*]	MO[†]	CN[‡]	B_0 [*]	B_V				
	GPa								MPa·m$^{1/2}$
rh-BN	56	72	67	382	369	389 (G_V)	864	0.110	4.6
rh-B_2N_2 [22]	55	75	73	375	356	400 (G_V)	873	0.091	4.4
w-BN	54	70	64	374[**]		384[††]	858	0.118	4.7
c-BN	55	74	69	377[**]		402[‡‡]	890	0.107	4.8

[*] Thermodynamic model [17]

[†] Mazhnik-Oganov model [15]

[‡] Chen-Niu model [16]

[§] E and ν values calculated using isotropic approximation

[**] Ref. 25

[††] Ref. 26

[‡‡] Ref. 27

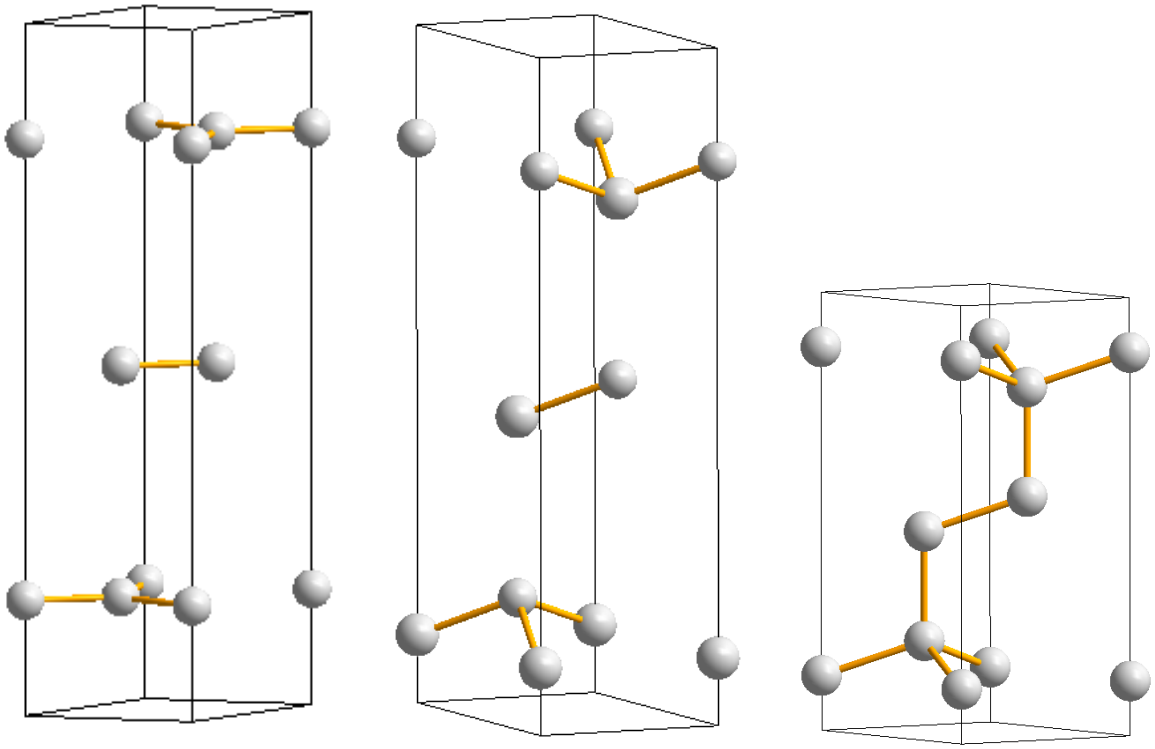

(*a*) (*b*) (*c*)

Figure 1. Transformation mechanism using hexagonal setting of rhombohedral structures. (*a*) 2D 3*R* graphite with C(sp^2), $z(C) \sim 0.167$; (*b*) with $z(C) = 0.125$ a non-relaxed intermediate phase is obtained with three non-planar puckered layers; (*c*) fully relaxed 3D new phase with tetrahedral sp^3 carbon alike diamond resulting into a much more compact structure with smaller *c* hexagonal parameter. The ∠C–C–C angle changes from (*a*) 120° (sp^2) to (*b*) 96°, and (*c*) 109.47° (sp^3).

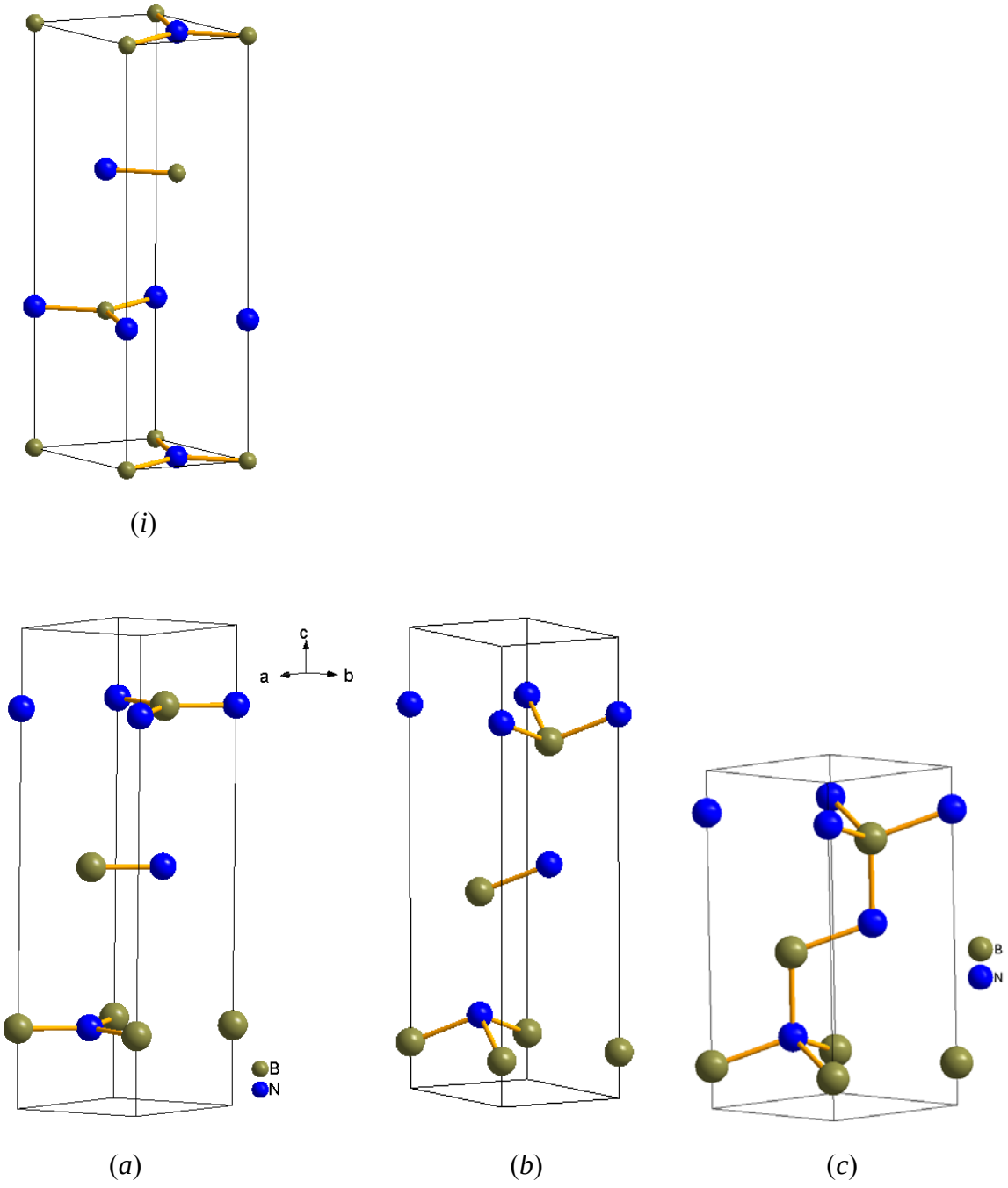

Figure 2. Transformation mechanism using hexagonal setting of rhombohedral BN structures in hexagonal settings. (*i*) *rh*-BN 3R from Ref. [5], not retained herein as model. (*a*) B_3N_3 with z(B) = 0.167 and z(N) = 0.833; (*b*) non-relaxed intermediate phase with three non-planar layers, and (*c*) fully relaxed 3D new BN (B_3N_3) with *BN3* and *NB3* tetrahedra resulting into a much more 3D compact structure.

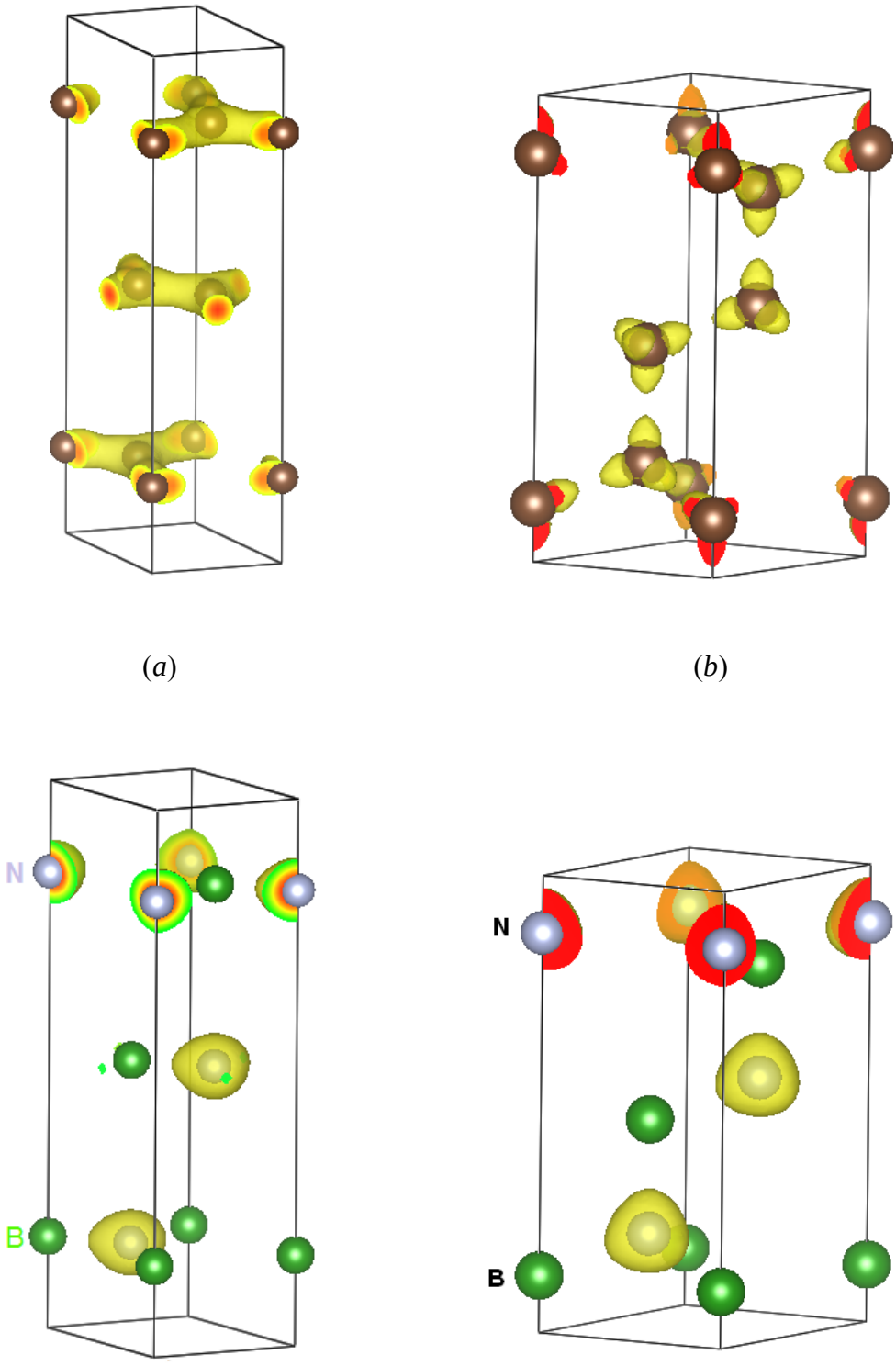

(*a*) (*b*)

(*c*) (*d*)

Figure 3. Charge densities of the rhombohedral structures in hexagonal settings. (*a*) C_6 3*R*, (*b*) 3D C_6, (*c*) B_3N_3 3*R*, (*d*) 3D B_3N_3

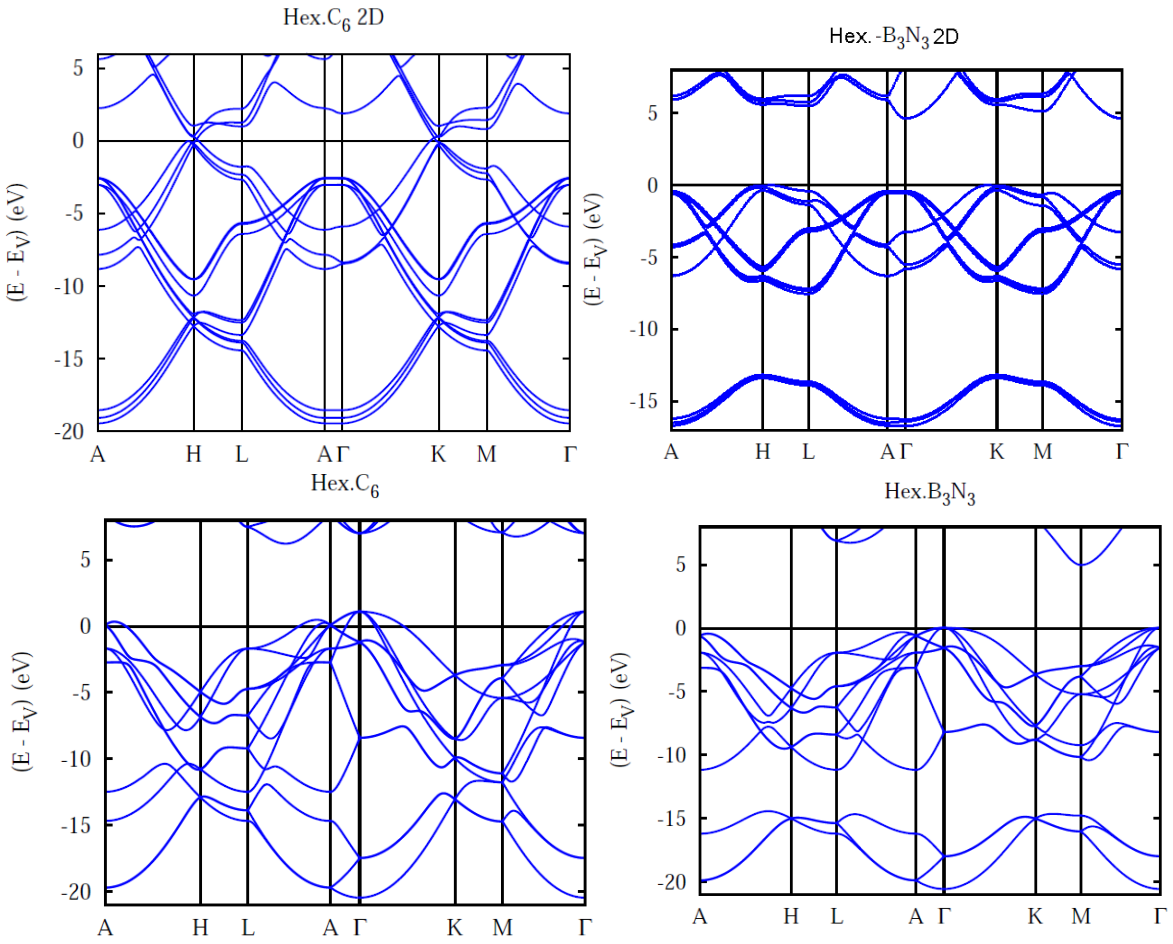

Figure 4. Electronic band structures of 2D (top) and 3D (bottom) new rhombohedral forms of carbon and boron nitride.